SIAM J. SCI. COMPUT.
Vol. 37, No. 1, pp. A271–A294

LONG TIME NUMERICAL SIMULATIONS FOR PHASE-FIELD PROBLEMS USING *P*-ADAPTIVE SPECTRAL DEFERRED CORRECTION METHODS*

XINLONG FENG†, TAO TANG‡, AND JIANG YANG‡

Abstract. A high-order and energy stable scheme is developed to simulate phase-field models by combining the semi-implicit spectral deferred correction (SDC) method and the energy stable convex splitting technique. The convex splitting scheme we use here is a linear unconditionally stable method but is only of first-order accuracy, so the SDC method can be used to iteratively improve the rate of convergence. However, it is found that the accuracy improvement may affect the overall energy stability which is intrinsic to the phase-field models. To compromise the accuracy and stability, a local p-adaptive strategy is proposed to enhance the accuracy by sacrificing some local energy stability in an acceptable level. The proposed strategy is found very useful for producing accurate numerical solutions at small time (dynamics) as well as long time (steady state) with reasonably large time stepsizes. Numerical experiments are carried out to demonstrate the high effectiveness of the proposed numerical strategy.

Key words. semi-implicit spectral deferred correction methods, energy stable convex splitting, phase-field models, adaptive scheme, long time simulation

AMS subject classifications. 65M06, 65M12

DOI. 10.1137/130928662

1. Introduction.

The phase-field method is very useful for modeling interfacial phenomena. Phase-field models take two distinct values (for instance, $+1$ and -1) in each of the phases, with a smooth change between both values in the zone around the interface, which is then diffused with a finite width. The phase-field method was first used to describe the microstructure evolution [7, 16] and phase transition [21, 25, 30, 36], but it has been recently extended to many other physical phenomena, such as solid-solid transitions, growth of cancerous tumors, phase separation of block copolymers, dewetting and rupture of thin liquid films, and infiltration of water into a porous medium.

Three of these phase-field models have attracted much attention: the Allen–Cahn equation,

$$\frac{\partial u}{\partial t} = \epsilon^2 \Delta u - f(u), \quad \mathbf{x} \in \Omega,\ t \in (0, T], \tag{1.1}$$

$$u(\mathbf{x}, 0) = u_0(\mathbf{x}), \quad \mathbf{x} \in \bar{\Omega}; \tag{1.2}$$

*Submitted to the journal's Methods and Algorithms for Scientific Computing section July 11, 2013; accepted for publication (in revised form) November 3, 2014; published electronically January 29, 2015.

http://www.siam.org/journals/sisc/37-1/92866.html

†College of Mathematics and System Sciences, Xinjiang University, Urumqi 830046, People's Republic of China, and Institute of Theoretical and Computational Studies and Department of Mathematics, Hong Kong Baptist University, Kowloon Tong, Hong Kong (fxlmath@gmail.com). The research of this author was supported in part by the Hong Kong Scholars Program and the National Science Foundation of China.

‡Institute of Theoretical and Computational Studies and Department of Mathematics, Hong Kong Baptist University, Kowloon Tong, Hong Kong (ttang@hkbu.edu.hk, jyanghkbu@gmail.com). The research of the second author was supported in part by Hong Kong Research Grants Council CERG grants, the National Science Foundation of China, and Hong Kong Baptist University FRG grants. The research of the third author was supported in part by the Hong Kong Research Grants Council and Hong Kong Baptist University.

the Cahn–Hilliard equation,

$$\frac{\partial u}{\partial t} = \Delta(-\epsilon^2 \Delta u + f(u)), \quad \mathbf{x} \in \Omega,\ t \in (0, T], \tag{1.3}$$

$$u(\mathbf{x}, 0) = u_0(\mathbf{x}), \quad \mathbf{x} \in \bar{\Omega}; \tag{1.4}$$

and the thin film model (also called the molecular beam epitaxy (MBE) model without slope selection),

$$\frac{\partial u}{\partial t} = -\epsilon^2 \Delta^2 u + \nabla \cdot f(\nabla u), \quad \mathbf{x} \in \Omega,\ t \in (0, T], \tag{1.5}$$

$$u(\mathbf{x}, 0) = u_0(\mathbf{x}), \quad \mathbf{x} \in \bar{\Omega}. \tag{1.6}$$

For simplicity, we impose periodic boundary conditions or homogeneous Neumann boundary conditions for all three equations. Here Ω is a bounded domain in $\mathcal{R}^2$ and T is a finite time. In both (1.1) and (1.3), u represents the concentration of one of the two metallic components of the alloy, and the parameter ϵ^2 represents the interfacial width, which is small compared to the characteristic length of the laboratory scale. In the thin film model (1.5), u is a scaled height function of epitaxial growth of thin films in a co-moving frame. The three models can be viewed as the gradient flow associated with the following energy functions, respectively:

$$E(u) = \int_\Omega \left(\frac{1}{2} \epsilon^2 |\nabla u|^2 + F(u) \right) dx \tag{1.7}$$

in L^2 for the Allen–Cahn equation,

$$E(u) = \int_\Omega \left(\frac{1}{2} \epsilon^2 |\nabla u|^2 + F(u) \right) dx \tag{1.8}$$

in H^{-1} for the Cahn–Hilliard equation, and

$$E(u) = \int_\Omega \left(\frac{1}{2} \epsilon^2 |\Delta u|^2 + F(\nabla u) \right) dx \tag{1.9}$$

for the thin film model both with and without slope selection, where $F(u)$ is a given energy potential and $f(u) = F'(u)$ is usually a nonlinear term in these equations. The nonlinear term taken here is the double well potential

$$F(u) = \frac{1}{4}(u^2 - 1)^2, \quad f(u) = u^3 - u, \tag{1.10}$$

for the Allen–Cahn equation and the Cahn–Hilliard equation as in most of the literature. For the thin film models with slope selection,

$$F(\nabla u) = \frac{1}{4}(|\nabla u|^2 - 1)^2, \quad f(\nabla u) = -(1 - |\nabla u|^2)\nabla u, \tag{1.11}$$

and for the thin film models without slope selection,

$$F(\nabla u) = -\frac{1}{2} \ln(|\nabla u|^2 + 1), \quad f(\nabla u) = -\frac{\nabla u}{1 + |\nabla u|^2}. \tag{1.12}$$

Enormous efforts on numerical simulations and numerical analysis have been made for these equations. For temporal discretization, the numerical methods can be classified into explicit schemes (linear schemes), implicit schemes (nonlinear schemes),

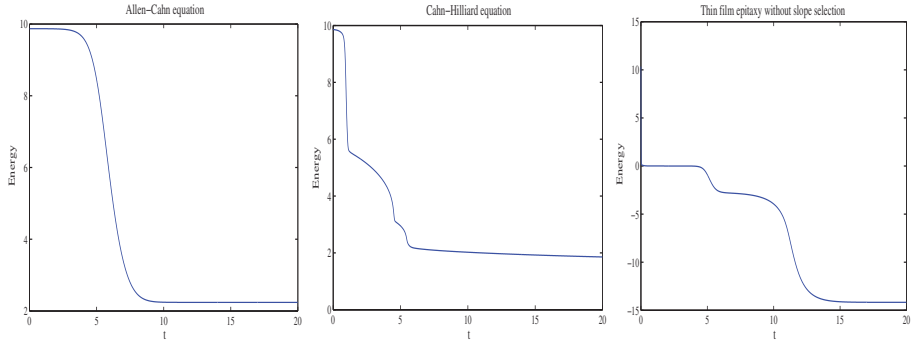

FIG. 1. *Illustrative energy curves of the three different models.*

and implicit-explicit schemes. In general, the implicit-explicit approach is found to be more powerful in terms of accuracy and stability for the phase-field models; see, e.g., [15, 23, 34, 38]. In particular, the schemes presented in [23, 33, 34, 37, 38] are shown to be nonlinearly energy stable. The nonlinear schemes usually take some special treatments for the nonlinear terms (see, e.g., [13, 20, 31, 39]), which require some simple iterations to solve the resulting nonlinear system in each time step. It is noted that for phase-field type problems Kassam and Trefethen [24] use the exponential time-differencing fourth-order Runge–Kutta method for temporal discretization, which has been demonstrated to be a powerful technique.

As the governing equations (1.3) and (1.5) involve the perturbed (i.e., the coefficient $\epsilon^2 \ll 1$) biharmonic operators and strong nonlinearities, it is very difficult to design an efficient time discretization strategy which can resolve dynamics and steady state of the corresponding phase-field models. Moreover, nonlinear energy stability which is intrinsic to the phase-field models (see, e.g., Figure 1) is also a challenging issue for numerical approximations. Numerical evidence shows that violating the energy stability may lead to nonphysical oscillations. Consequently, a satisfactory numerical strategy needs to balance solution accuracy, efficiency, and nonlinear stability.

Among the time discretizations concerning nonlinear stability, Eyre's [17] convex splitting scheme should be specially mentioned. It is a first-order accurate unconditionally stable time-stepping scheme for gradient flows, which can be either linear or nonlinear depending on the ways of splitting. In particular, it has served as inspiration for many other time integration schemes in recent years; see, e.g., [4, 6, 11, 18, 19]. The starting point of our work is also based on the convex splitting scheme. Moreover, explicit schemes may have stability problems and fully nonlinear schemes require nonlinear iterations at each time step. As we are interested in small and large time simulations, the linear implicit-explicit schemes are within our consideration. More precisely, we will first consider a linear implicit-explicit scheme by using the convex splitting idea.

Below we will briefly outline the motivation and main findings of this work. Our numerical evidence shows that the lower-order time discretizations may require very small time stepsizes in order to resolve the short time dynamics of the phase-field problems. Figure 2 gives a typical example which gives energy evolutions for the Cahn–Hilliard problem (1.3)–(1.4) with $\Delta t = 1/1000, 1/100, 1/50$. It is observed that a time step smaller than 10^{-2} is needed in order to obtain accurate solutions.

For improvement, one quick idea is to use higher-order time discretization. However, there are no higher-order energy-stable schemes, particularly for order 3 or

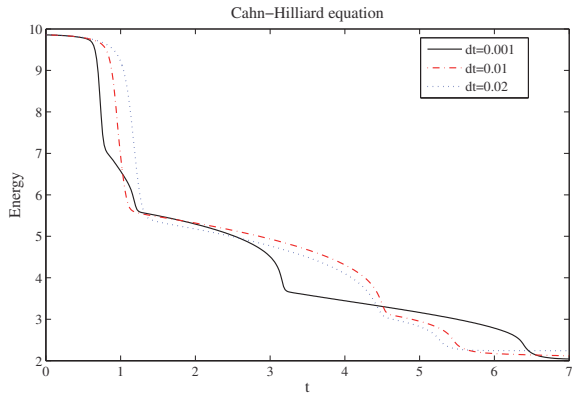

FIG. 2. *A typical example for the energy dependent on time steps for the Cahn–Hilliard equation. A detail description of the example can be found in section* 6.

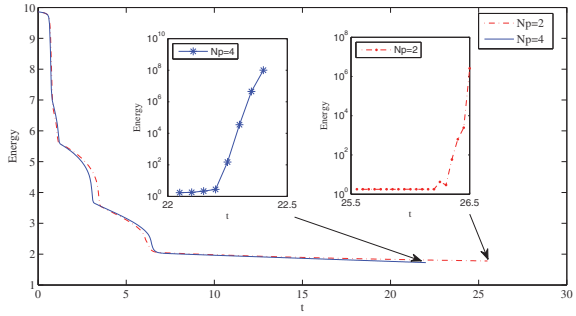

FIG. 3. *A typical energy blow-up with third- (right) or fifth- (left) order time discretization for the Cahn–Hilliard equation.*

higher. Our idea is to use the so-called spectral deferred correction (SDC) method which was first introduced to solve initial value ordinary differential equations (ODEs) by Dutt, Greengard, and Rokhlin [14]. The key idea of the SDC method is to first convert the original ODEs into the corresponding Picard equation and then apply a deferred correction procedure in the integral formulation, aiming to achieve higher-order accuracy in an *iterative* way. The reasons for us to employ the SDC method are the following: iteration loops can improve the formal accuracy in a flexible and simple way; the SDC method was designed to handle stiff systems which are the case of our perturbed singularly nonlinear equations; and the flexibility of the order enhancement is useful for our local adaptive strategy to be described later. On the other hand, although the SDC method can solve the short time dynamics very well (e.g., a fifth-order time discretization can fix the problem in Figure 2 with $\Delta t = 1/20$), unfortunately, a higher-order time discretization may yield numerical instability as the nonlinear stability cannot be guaranteed for higher-order time discretizations. A typical example is given in Figure 3, which solves the same example as in Figure 2 but with a third order SDC method (i.e., $Np = 2$ in the figure) and a fifth-order SDC method (i.e., $Np = 4$). It is observed that the discrete energies blow up before $T = 30$.

To fix the problems in Figures 2 and 3, we will propose a hybrid p-adaptive method which chooses the appropriate order of accuracy at each time level. It is seen

from the energy curves in Figure 1 that first-order methods should be good enough in most time regimes, but in some critical stages with rapid energy change appropriate adaptive strategies must be used. Some p-adaptive details will be reported and the relevant numerical results will be presented in this work. It will be demonstrated that the adaptive procedure is robust and effective for simulating both dynamics and steady state of the phase-field problems.

The rest of this paper is organized as follows. In section 2, three energy convex splitting schemes are constructed, which are semi-implicit and unconditionally stable for the Allen–Cahn equation, the Cahn–Hilliard equation, and the thin film models. We will give some direct energy stability proof without applying the general result of Eyre [17]. In section 3 we give a brief review on the SDC method, and in section 4 we adopt a fast Poisson solver for handling the Laplace operators. A simple but useful p-adaptive strategy will be proposed in section 5. Numerical experiments will be carried out in section 6, and some concluding remarks will be given in the final section.

2. Energy stability with convex splitting. In [17], Eyre gives an unconditionally stable time-stepping scheme for general gradient systems. As the underlying models are gradient flows associated with the free energy, it is natural to extend Eyre's work to these models.

For ease of notation, we denote the free energy in (1.7)–(1.9) as $E(u) = \int_\Omega G(u)dx$. The key idea of energy convex splitting is to split the functional $G(u)$ into the difference of two strictly convex functions: contractive term $G_c(u)$ and expansive term $G_e(u)$, i.e.,

$$E(u) = E_c(u) - E_e(u) = \int_\Omega G_c(u)dx - \int_\Omega G_e(u)dx. \tag{2.1}$$

This decomposition must satisfy the requirement that all eigenvalues of $J(\nabla G_e(u))$ dominate the largest eigenvalue of $-J(\nabla G(u))$.

The ways to split the energy function are not unique, and the resulting scheme may be implicit, which requires a couple of iterations. For our purpose, we wish to design linear energy stable schemes. Inspired by the energy splitting method in [4], we will construct linear unconditionally stable schemes for the phase-field models under investigation.

2.1. A linear energy stable convex splitting scheme for the Allen–Cahn equation. The Allen–Cahn equation is a gradient flow in L^2 with the free energy (1.7). It can be verified that the following splitting satisfies the standard convex splitting conditions:

$$E_c(u) = \int_\Omega \left(\frac{\epsilon^2}{2}|\nabla u|^2 + \frac{\beta}{2}u^2\right) dx, \quad E_e(u) = \int_\Omega \left(\frac{\beta}{2}u^2 - F(u)\right) dx, \tag{2.2}$$

where $E_c(u)$ and $E_e(u)$ represent the contractive term and the expansive term, respectively, and the free parameter β is a sufficiently large constant. The corresponding numerical scheme to this energy splitting with time step k is given by

$$\begin{aligned} \frac{u^{n+1} - u^n}{k} &= -\left(\frac{\delta E_c(u^{n+1})}{\delta u} - \frac{\delta E_e(u^n)}{\delta u}\right) \\ &= \epsilon^2 \Delta u^{n+1} - \beta u^{n+1} + \beta u^n - f(u^n). \end{aligned} \tag{2.3}$$

THEOREM 2.1. *For the Allen–Cahn equation* (1.1), *if the boundary values and the initial value are both bounded by* 1, *then the semidiscrete scheme* (2.3) *with* $\beta \geq 2$ *is unconditionally energy stable, i.e., for all* $k > 0$,

$$E(u^{n+1}) \leq E(u^n), \quad n = 0, 1, \ldots, \tag{2.4}$$

where the energy E *is defined by* (1.7).

Proof. We first prove that the nimerical solution generated by (2.3) is bounded by 1. To this end, we first notice that the scheme (2.3) can be rewritten as

$$(1 + \beta k)u^{n+1} - k\epsilon^2 \Delta u^{n+1} = (1 + \beta k)u^n + k(u^n - (u^n)^3), \tag{2.5}$$

where we have used the expression for $f(u)$, i.e., (1.10). Denote

$$g(x) = (1 + \beta k)x + k(x - x^3). \tag{2.6}$$

If $\beta \geq 2$, then it is easy to verify that

$$\max_{|x|\leq 1} g(x) = g(1) = 1 + \beta k; \quad \min_{|x|\leq 1} g(x) = g(-1) = -(1 + \beta k). \tag{2.7}$$

We will use mathematical induction to show that $\|u^m\|_\infty$ is bounded by 1 for all potitive integers m. This is true for $m = 0$ by the assumption on the initial data. Assume the claim is true on the time level t_n, i.e.,

$$\|u^n\|_\infty \leq 1. \tag{2.8}$$

If u^{n+1} achieves the maximum at $x^* \in \Omega$, then $\Delta u^{n+1}(x^*) \leq 0$. This, together with (2.5), gives

$$(1 + \beta k) \max(u^{n+1}) \leq g(u^n(x^*)) \leq 1 + \beta k, \tag{2.9}$$

where in the last step we have used (2.7) and (2.8). The above result leads to $\|u^{n+1}) \leq 1$. Similarly, we can show that $\min(u^{n+1}) \geq -1$. Note that the boundary values are bounded by 1. Then we have proved that $\|u^{n+1}\|_\infty \leq 1$ in $\bar{\Omega}$. This established the maximum principle for the scheme (2.3).

Taking the energy difference between two consecutive time levels and expanding $F(u)$ by Taylor expansion yield

$$\begin{aligned} E(u^{n+1}) - E(u^n) = {} & \frac{\epsilon^2}{2}\Big(||\nabla u^{n+1}||_2^2 - ||\nabla u^n||_2^2\Big) + (f(u^n), u^{n+1} - u^n) \\ & + \frac{1}{2}(f'(\xi_n)(u^{n+1} - u^n), u^{n+1} - u^n), \end{aligned} \tag{2.10}$$

where $f'(\xi_n) = 1 - 3\xi_n^2$ and ξ_n lies between u^n and u^{n+1}. The maximum principle established above suggests that $|\xi_n| \leq 1$, which gives $|f'(\xi_n)| \leq 2$. Consequently, (2.10) can be estimated as

$$E(u^{n+1}) - E(u^n) \leq \frac{\epsilon^2}{2}\Big(||\nabla u^{n+1}||_2^2 - ||\nabla u^n||_2^2\Big) + (f(u^n), u^{n+1} - u^n) + ||u^{n+1} - u^n||_2^2. \tag{2.11}$$

Taking the L^2 inner product of (2.3) with $u^{n+1} - u^n$, we get

$$\begin{aligned} & \frac{||u^{n+1} - u^n||_2^2}{k} \\ & \quad = \epsilon^2(\Delta u^{n+1}, u^{n+1} - u^n) - \beta||u^{n+1} - u^n||_2^2 - (f(u^n), (u^{n+1} - u^n)) \\ & \quad =: I_1 - \beta||u^{n+1} - u^n||_2^2 - (f(u^n), u^{n+1} - u^n). \end{aligned} \tag{2.12}$$

It can be shown that

$$I_1 = -\frac{\epsilon^2}{2}\Big(||\nabla u^{n+1}||_2^2 - ||\nabla u^n||_2^2 + ||\nabla u^{n+1} - \nabla u^n||_2^2\Big). \tag{2.13}$$

Substituting the above expression into (2.12) yields

$$\begin{aligned} -\frac{\epsilon^2}{2}||\nabla u^{n+1} - \nabla u^n||_2^2 &= \frac{\epsilon^2}{2}\Big(||\nabla u^{n+1}||_2^2 - ||\nabla u^n||_2^2\Big) \\ &+ \left(\beta + \frac{1}{k}\right)||u^{n+1} - u^n||_2^2 + (f(u^n), u^{n+1} - u^n). \end{aligned} \tag{2.14}$$

Combining (2.11) and (2.14) gives

$$E(U^{n+1}) - E(U^n) \le -\frac{\epsilon^2}{2}||\nabla u^{n+1} - \nabla u^n||_2^2 + \left(1 - \beta - \frac{1}{k}\right)||u^{n+1} - u^n||_2^2. \tag{2.15}$$

Using the condition $\beta \ge 2$ leads to the desired energy decay result (2.4). ∎

The above result seems new in the sense that the constant β can be bounded uniformly by using the maximum principle for the semidiscrete scheme. This makes the splitting scheme (2.3) theoretically reliable.

2.2. A linear energy stable convex splitting scheme for the Cahn–Hilliard equation. It is known that the Cahn–Hilliard equation is a gradient flow in H^{-1} with the free energy (1.8). Using the splitting form

$$E_c(u) = \int_\Omega \left(\frac{\epsilon^2}{2}|\nabla u|^2 + \frac{\beta}{2}u^2\right) dx, \quad E_e(u) = \int_\Omega \left(\frac{\beta}{2}u^2 - F(u)\right) dx, \tag{2.16}$$

where F is given by (1.10), the corresponding semidiscrete scheme to the Cahn–Hilliard equation is

$$\begin{aligned} \frac{u^{n+1} - u^n}{k} &= \Delta\left(\frac{\delta E_c(u^{n+1})}{\delta u} - \frac{\delta E_e(u^n)}{\delta u}\right) \\ &= -\epsilon^2\Delta^2 u^{n+1} + \beta\Delta u^{n+1} - \beta\Delta u^n + \Delta f(u^n). \end{aligned} \tag{2.17}$$

THEOREM 2.2. *For the Cahn–Hilliard equation, if the constant β in* (2.17) *is sufficiently large, then the semidiscrete scheme* (2.17) *is unconditionally energy stable, i.e.,*

$$E(u^{n+1}) \le E(u^n), \quad n = 0, 1, \ldots, \tag{2.18}$$

where the energy E is defined by (1.8)*. Moreover, if the numerical solution is convergent in $L^\infty([0,T], W^{1,\infty}(\Omega))$ as $k \to 0$, then the size of the constant β can be controlled by*

$$\beta \sim \frac{1}{2}\max_{|v| \le \|u\|_\infty} |f'(v)|. \tag{2.19}$$

Proof. We use $||\cdot||_2$ to denote the L^2 norm and $(\cdot,\cdot)$ to the inner product in L^2. Taking the energy difference between two consecutive time levels and expanding $F(u)$ by Taylor expansion yield

$$
\begin{aligned}
E(u^{n+1}) - E(u^n) &= \frac{\epsilon^2}{2}\Big(||\nabla u^{n+1}||_2^2 - ||\nabla u^n||_2^2\Big) \\
&\quad + (f(u^n), u^{n+1} - u^n) + \frac{1}{2}(f'(\xi_n)(u^{n+1} - u^n), u^{n+1} - u^n) \\
&\le \frac{\epsilon^2}{2}\Big(||\nabla u^{n+1}||_2^2 - ||\nabla u^n||_2^2\Big) \\
&\quad + (f(u^n), u^{n+1} - u^n) + \frac{\alpha_n}{2}||u^{n+1} - u^n||_2^2, \qquad (2.20)
\end{aligned}
$$

where

$$
\alpha_n := \max\Big\{\|f'(u^n)\|_\infty, \|f'(u^{n+1})\|_\infty, 1\Big\}. \qquad (2.21)
$$

Rewrite the scheme (2.17) as

$$
u^{n+1} - u^n = k\Delta\eta, \qquad (2.22a)
$$

$$
\eta = -\epsilon^2\Delta u^{n+1} + \beta u^{n+1} - \beta u^n + f(u^n). \qquad (2.22b)
$$

Assume that

$$
\beta \ge \frac{1}{2}\alpha_n. \qquad (2.23)
$$

Taking the L^2 inner product for (2.22a) with η and combining (2.20) yield

$$
\begin{aligned}
&(\eta, u^{n+1} - u^n) = -k||\nabla\eta||_2^2 \\
&= (-\epsilon^2\Delta u^{n+1} + \beta u^{n+1} - \beta u^n + f(u^n), u^{n+1} - u^n) \\
&= \epsilon^2(\nabla u^{n+1}, \nabla u^{n+1} - \nabla u^n) + \beta||u^{n+1} - u^n||_2^2 + (f(u^n), u^{n+1} - u^n) \\
&\ge \tfrac{\epsilon^2}{2}\left(||\nabla u^{n+1}||_2^2 - ||\nabla u^n||_2^2\right) + \tfrac{\alpha_n}{2}||u^{n+1} - u^n||_2^2 + (f(u^n), u^{n+1} - u^n) \\
&\quad + \tfrac{\epsilon^2}{2}||\nabla u^{n+1} - \nabla u^n||_2^2 \\
&\ge E(u^{n+1}) - E(u^n) + \tfrac{\epsilon^2}{2}||\nabla u^{n+1} - \nabla u^n||_2^2,
\end{aligned}
$$

where in the second to last step we have used (2.23). Consequently, we have

$$
E(u^{n+1}) - E(u^n) \le -k||\nabla\eta||_2^2 - \frac{\epsilon^2}{2}||\nabla u^{n+1} - \nabla u^n||_2^2 \le 0,
$$

which is the desired result (2.18). If the numerical solution is convergent in $L^\infty([0,T], W^{1,\infty}(\Omega))$ as $k \to 0$, then combining (2.21) and (2.23) gives (2.19). ∎

2.3. A linear energy stable convex splitting scheme for the MBE model. It is known that the thin film model is a gradient flow in L^2 with the free energy (1.9). In this case, using the convex splitting

$$
E_c(u) = \int_\Omega \left(\frac{\epsilon^2}{2}|\Delta u|^2 + \frac{\beta}{2}|\nabla u|^2\right) dx, \quad E_e(u) = \int_\Omega \left(\frac{\beta}{2}|\nabla u|^2 - F(\nabla u)\right) dx, \qquad (2.24)
$$

gives the corresponding semidiscrete scheme

$$
\begin{aligned}
\frac{u^{n+1} - u^n}{k} &= -\left(\frac{\delta E_c(u^{n+1})}{\delta u} - \frac{\delta E_e(u^n)}{\delta u}\right) \\
&= -\epsilon^2\Delta^2 u^{n+1} + \beta\Delta u^{n+1} - \beta\Delta u^n + \nabla\cdot f(\nabla u^n). \qquad (2.25)
\end{aligned}
$$

THEOREM 2.3. *For the semidiscrete scheme* (2.25)*, we have the following results:*

(i) *For the thin film model* (1.5) *with slope selection* (1.11)*, if the constant* β *in* (2.25) *is sufficiently large, then* (2.25) *is unconditionally energy stable in the sense of* $E(u^{n+1}) \le E(u^n)$*, where the energy* E *is defined by* (1.9).

(ii) *For the thin film model* (1.5) *without slope selection* (1.12)*, if the constant* β *in* (2.25) *satisfies* $\beta \ge \frac{1}{2}$*, then* (2.25) *is unconditionally energy stable in the sense of* $E(u^{n+1}) \le E(u^n)$*, where the energy* E *is defined by* (1.9).

Proof. The proof of part (i) is similar to the proof of the last theorem and we will omit it here. For the thin film model (1.5) without slope selection (1.12), we observe that

$$||\partial^2_{\nabla u} F(\nabla u)||_2 = \frac{1}{1+|\nabla u|^2} \le 1.$$

Note that

$$f(\nabla u) = \partial_{\nabla u} F(\nabla u) \quad \text{and} \quad \partial_{\nabla u} f(\nabla u) = \partial^2_{\nabla u} F(\nabla u).$$

Consequently, for all u we have

$$\max_{u \text{ solves MBE}} ||\partial_{\nabla u} f(\nabla u)||_2 \le 1. \tag{2.26}$$

Similar to (2.20), we obtain from (2.25) and (2.26) that

$$\begin{aligned} E(u^{n+1}) - E(u^n) \le & \frac{\epsilon^2}{2}\left(||\Delta u^{n+1}||_2^2 - ||\Delta u^n||_2^2\right) \\ & + (f(\nabla u^n), \nabla(u^{n+1}-u^n)) + \frac{1}{2}||\nabla(u^{n+1}-u^n)||_2^2. \end{aligned} \tag{2.27}$$

Taking the L^2 inner product of (2.25) with $u^{n+1}-u^n$ yields

$$\begin{aligned} & \frac{||u^{n+1}-u^n||_2^2}{k} \\ & = (-\epsilon^2\Delta^2 u^{n+1} + \beta\Delta u^{n+1} - \beta\Delta u^n + \nabla\cdot f(\nabla u^n), u^{n+1}-u^n) \\ & = -\epsilon^2(\Delta u^{n+1}, \Delta u^{n+1} - \Delta u^n) - \beta||\nabla(u^{n+1}-u^n)||_2^2 - (f(\nabla u^n), \nabla(u^{n+1}-u^n)) \\ & =: I_1 - \beta||\nabla(u^{n+1}-u^n)||_2^2 - (f(\nabla u^n), \nabla(u^{n+1}-u^n)). \end{aligned} \tag{2.28}$$

It can be shown that

$$I_1 = -\frac{\epsilon^2}{2}\Big(||\Delta u^{n+1}||_2^2 - ||\Delta u^n||_2^2 + ||\Delta u^{n+1} - \Delta u^n||_2^2\Big). \tag{2.29}$$

Using (2.27)–(2.29) and the assumption $\beta \ge \frac{1}{2}$ yields

$$\frac{||u^{n+1}-u^n||_2^2}{k} \le -\left(E(u^{n+1}) - E(u^n) + \frac{\epsilon^2}{2}||\nabla u^{n+1} - \nabla u^n||_2^2\right),$$

which leads to

$$E(u^{n+1}) - E(u^n) \le -\frac{||u^{n+1}-u^n||_2^2}{k} - \frac{\epsilon^2}{2}||\nabla u^{n+1} - \nabla u^n||_2^2 \le 0. \tag{2.30}$$

This proves part (ii) of the theorem. ∎

In practical computations, for the Cahn–Hilliard equation and the MBE equation with slope selection, the assumption that β is sufficiently large can be relaxed. For example, take the double well potential $F(u) = \frac{1}{4}(u^2-1)^2$ with $|f'(u)| = |3u^2-1|$. As the physical solution u is bounded in $[-1,1]$, the condition (2.19) implies that $\beta = 1$ is big enough for the stability. Similarly, for the MBE model with selection, $\beta = 2$ will be sufficient for the stability. This is indeed confirmed by our numerical computations.

For the MBE equation without slope selection, the clean condition of $\beta \geq \frac{1}{2}$ is due to the boundedness of (2.26). A similar observation of this nice property is also made and used in [8, 9].

3. SDC schemes and semi-implicit SDC schemes. The SDC was first introduced to solve the Cauchy problem for ODEs by Dutt, Greengard, and Rokhlin in [14]. The key idea of the SDC method is to convert the original ODEs into the corresponding Picard equation and then apply a deferred correction procedure in the integral formulation. The goal of the SDC method is to achieve higher-order accuracy schemes for both nonstiff and stiff problems. Below we briefly describe the SDC method.

Consider the following ODE system:

$$\begin{aligned} &u'(t) = G(t,u(t)), \quad t \in (a,b], \\ &u(a) = u_a, \end{aligned} \tag{3.1}$$

where $u(t), u_a \in R^n$, and $G : [a,b] \times R^n \to R^n$. It is assumed that G is sufficiently smooth so that the discussion of higher-order methods is appropriate.

The corresponding Picard integral equation to (3.1) is

$$u(t) = u_a + \int_a^t G(\tau, u(\tau))d\tau. \tag{3.2}$$

Given an initial approximation to the solution $u^0(t)$, a residual function to measure the quality of the approximation is defined as follows:

$$\epsilon(t,u^0) = u_a + \int_a^t G(\tau, u^0(\tau))d\tau - u^0(t). \tag{3.3}$$

By denoting the error function by $\delta(t) = u(t) - u^0(t)$ and substituting $u(t) = u^0(t) + \delta(t)$ into (3.2), we obtain

$$\delta(t) = u_a + \int_a^t G(\tau, u^0(\tau) + \delta(\tau))d\tau - u^0(t). \tag{3.4}$$

Subtracting (3.3) from (3.4) gives

$$\delta(t) = \int_a^t G(\tau, u^0(\tau) + \delta(\tau)) - G(\tau, u^0(\tau))d\tau + \epsilon(t). \tag{3.5}$$

Equation (3.5) is referred to as the correction equation. After using some numerical method to discretize the correction equation (3.5), such as the explicit Euler method for non-stiff problems or the implicit Euler method for stiff problems, and adding the error function $\delta(t)$ to the initial approximation $u^0(t)$, we can get higher-order approximated solution $u^c(t)$, where $u^c(t) = u^0(t) + \delta(t)$. In the following subsections, we present this procedure in more detail.

3.1. SDC methods based on Euler methods. First we divide the computational time interval $[0,T]$ into N nonoverlapping intervals $0=t_0<t_1<\cdots<t_N=T$. We do the SDC procedure in every interval $[t_n,t_{n+1}]$. Denoting the $p+1$ Legendre–Guass–Radau IIa nodes (cf. [32]) on $[-1,1]$ by $-1=r_0<r_1<\cdots<r_{p-1}<r_p=1$ and letting

$$\tau_i=\frac{t_{n+1}-t_n}{2}r_i+\frac{t_{n+1}+t_n}{2},\quad i=0,1,\ldots,p,$$

we obtain the spectral nodes on interval $[t_n,t_{n+1}]$ of the form $t_n=\tau_0<\tau_1<\cdots<\tau_{p-1}<\tau_p=t_{n+1}$. Then the interval $[t_n,t_{n+1}]$ is divided into p subintervals, i.e., $[t_n,t_{n+1}]=\bigcup_{i=0}^{p-1}[\tau_i,\tau_{i+1}]$.

For convenience, we use the notation $u_i=u(\tau_i)$ (similarly for δ_i, $\epsilon_i(u^0)$) and $\Delta\tau_i=\tau_{i+1}-\tau_i$, and we take u_i^0 to represent the initial approximation at τ_i and u_i^c to represent the corrected approximation at τ_i. After obtaining numerical approximations at these spectral nodes $u_0^0,u_1^0,\ldots,u_p^0$ by the energy convex splitting scheme given in section 2, we can then compute the corrections δ_i to increase the accuracy for u^0 by $u_i^c=u_i^0+\delta_i$. One feasible way to discretize the correction equation (3.5) is the implicit Euler method as the phase-field models are usually stiff problems.

To be more specific, we set $u_0^c=u_0^0$ and $\delta_0=0$ as the initial value. Discretizing the correction equation (3.5) via the implicit Euler method, we have

$$\delta_{i+1}=\delta_i+\Delta\tau_i[G(\tau_{i+1},u_{i+1}^0+\delta_{i+1})-G(\tau_{i+1},u_{i+1}^0)]+\epsilon_{i+1}(u^0)-\epsilon_i(u^0). \tag{3.6}$$

Denote

$$I_i^{i+1}(u^0)=\int_{\tau_i}^{\tau_{i+1}}G(s,u^0(s))ds. \tag{3.7}$$

It follows from (3.3) that

$$I_i^{i+1}(u^0)=\epsilon_{i+1}(u^0)-\epsilon_i(u^0)+u_{i+1}^0-u_i^0. \tag{3.8}$$

Note $u_{i+1}^0+\delta_{i+1}=u_{i+1}^c$. Substituting the above equation into (3.6) gives

$$u_{i+1}^c=u_i^c+\Delta\tau_i[G(\tau_{i+1},u_{i+1}^c)-G(\tau_{i+1},u_{i+1}^0)]+I_i^{i+1}(u^0), \tag{3.9}$$

which gives an implicit equation for u^c. It remains to compute the integral (3.7) using the discrete values at the spectral nodes. One way is to approximate the continuous function $G(s,u^0)$ by using the Lagrange interpolation polynomials:

$$G_p(s,u^0)=\sum_{j=0}^{p}G(\tau_j,u_j^0)L_j^p(s), \tag{3.10}$$

where $L_j^p(s)$ is the Lagrange basis polynomial of degree p associate with the spectral points $\{\tau_j\}_{j=0}^p$. Approximate $I_i^{i+1}(u^0)$ by

$$I_i^{i+1}(u^0)\approx\int_{\tau_i}^{\tau_{i+1}}G_p(s,u^0(s))ds=\sum_{j=0}^{p}G(\tau_j,u_j^0)c_{ij}^p, \tag{3.11}$$

where

$$c_{ij}^p=\int_{\tau_i}^{\tau_{i+1}}L_j^p(s)ds. \tag{3.12}$$

If the correction procedure is implemented k times, we can enhance the order of accuracy for the approximation u^0 by $\min\{k,2p\}$ if $p+1$ Gauss–Radau nodes (including the two endpoints) are used (cf. [14, 35]).

3.2. Semi-implicit SDC methods. As the governing equations for phase-field models involving very small parameters, the resulting discretized equations may be very stiff. As a result, the explicit Euler method is not appropriate for the sake of the stability requirement. However, the conventional implicit Euler method leads to a nonlinear system, which affects the numerical efficiency. Note that the energy convex splitting scheme is essentially a semi-implicit scheme. This motivates us to use the semi-implicit Euler method. We can get extra benefit if we use the same explicit-implicit style in the energy convex splitting to solve the correction equation. That is to say, we split $G(s,u(s))$ into the implicit part $G_I(s,u(s))$ and the explicit part $G_E(s,u(s))$, and let $G_I(s,u(s)) = G_c(s,u(s))$ and $G_E(s,u(s)) = G_e(s,u(s))$, where $G_c(s,u(s))$ is the contractive term and $G_e(s,u(s))$ is the expansive term as given in section 2.

Similar to the last subsection, we derive the semi-implicit SDC for the correction equation (3.5) as

$$u_{i+1}^c = u_i^c + \Delta\tau_i[G_I(\tau_{i+1},u_{i+1}^c) - G_I(\tau_{i+1},u_{i+1}^0) + G_E(\tau_i,u_i^c) - G_E(\tau_i,u_i^0)] + I_i^{i+1}(u^0). \tag{3.13}$$

Below we just take the Cahn–Hilliard equation as an example to illustrate how to implement SDC to the phase-field models. To eliminate the ambiguity of notation, we denote time step $\Delta\tau_i = k$ in (2.17) and also let

$$G_I(s,u(s)) = G_c(s,u(s)) = -\epsilon^2\Delta^2 u + \beta\Delta u$$

and

$$G_E(s,u(s)) = G_e(s,u(s)) = -\beta\Delta u + \Delta f(u).$$

Then we get

$$\begin{aligned} u_{i+1}^c = u_i^c + k\Big((-\epsilon^2\Delta^2+\beta\Delta)u_{i+1}^c - (-\epsilon^2\Delta^2+\beta\Delta)u_{i+1}^0 \\ + (-\beta\Delta u_i^c + \Delta f(u_i^c)) - (-\beta\Delta u_i^0 + \Delta f(u_i^0))\Big) + I_i^{i+1}(u^0), \end{aligned} \tag{3.14}$$

which is given by scheme (2.17). To solve (3.14) for u^c, we only need to solve a linear system as the implicit term $F_I = F_c$ is linear. The key factor for solving the linear system efficiently is to handle the Laplace operators involved, which will be discussed in the next section.

We close this section by reviewing some convergence issues of the SDC method. We mention that the convergence for the SDC method on uniform quadrature nodes with high-order Runge–Kutta correction steps was established in [10] using a smoothness of rescaled error vector approach. With the same number of function evaluations, it was shown in [10] that the use of the higher-order integrators can have one magnitude of accuracy improvement. However, the order increase in the correction loop does not hold for nonuniform grids, e.g., the Gaussian quadrature nodes are excluded. In [35], a general framework for the convergence of the SDC method was established, which can recover high-order rate of convergence with nonuniform quadrature nodes. These theoretical results show that the SDC method not only is an ad hoc numerical strategy but also has a rigorous theoretical justification.

4. Spatial discretization and a fast Laplace solver. After discretizing governing equations in time as described in section 2, we end up with a general form of partial differential equations as follows:

$$u = -\gamma\Delta^2 u + \theta\Delta u + b, \tag{4.1}$$

where γ and θ are nonnegative constant parameters ($\gamma = 0$ is for the Allen–Cahn equation) and b is the given source term. Below we will use the central finite difference to discretize the Laplace operator.

Without loss of generality, we consider a computing domain $[0,1] \times [0,1]$ with mesh grid $\Delta x = \Delta y = h = \frac{1}{N}$. To simplify notation, let $u_{j,k} = u(x_j, y_k)$ and use $U = [u_{jk}]_{j=1,\dots N}^{k=1,\dots N}$ to represent the matrix of unknowns. The central difference scheme to approximate the Laplace operator is

$$\Delta u_{j,k} \approx \frac{u_{j-1,k} - 2u_{j,k} + u_{j+1,k}}{h^2} + \frac{u_{j,k-1} - 2u_{j,k} + u_{j,k+1}}{h^2} + \mathcal{O}(h^2). \tag{4.2}$$

By letting

$$M = \frac{1}{h^2}\begin{bmatrix} -2 & 1 & 0 & \cdots & 0 & 1 \\ 1 & -2 & 1 & 0 & \cdots & 0 \\ 0 & 1 & -2 & 1 & \cdots & 0 \\ \vdots & \vdots & \vdots & \vdots & \vdots & \vdots \\ 0 & \cdots & 0 & 1 & -2 & 1 \\ 1 & 0 & \cdots & 0 & 1 & -2 \end{bmatrix},$$

we can obtain from (4.2) the matrix form

$$\Delta U \approx UM + MU + \mathcal{O}(h^2). \tag{4.3}$$

Note that the matrix M is not strict tridiagonal as the top right and the lower left values are nonzero, which is due to the periodic boundary conditions. The matrix M is strict tridiagonal if the homogeneous Dirichlet boundary conditions are given. Similarly, we can get the matrix form for the biharmonic Laplace operator:

$$\Delta^2 U = \Delta(\Delta U) \approx (\Delta U)M + M(\Delta U) + \mathcal{O}(h^2) = M^2U + 2MUM + UM^2 + \mathcal{O}(h^2). \tag{4.4}$$

As M is a circulant matrix, it can be diagonalized by utilizing the unitary discrete Fourier transform matrix V_N (see, e.g., [12]):

$$V_N = \frac{1}{\sqrt{N}}F_N, \text{ where } F_N = (f_{jk}) \text{ with } f_{jk} = e^{-2jk\pi i/N}, \text{ for } 0 \le j,k < N.$$

In fact, we have

$$M = V_N^*\Lambda V_N, \text{ where } \Lambda = \operatorname{diag}(F_N \cdot c) = (\lambda_1, \dots, \lambda_N)^T \text{ and } c \text{ is the first column of } M.$$

Substituting the above diagonalized matrix into (4.3) and (4.4) and using the fact $V_N^*V_N = I_N$ yield

$$\Delta U \approx UV_N^*\Lambda V_N + V_N^*\Lambda V_N U + \mathcal{O}(h^2), \tag{4.5}$$

$$\Delta^2 U \approx V_N^*\Lambda^2 V_N U + 2V_N^*\Lambda V_N U V_N^*\Lambda V_N + UV_N^*\Lambda^2 V_N + \mathcal{O}(h^2). \tag{4.6}$$

Consequently, we obtain the discrete form for (4.1) with second-order accuracy:

$$U = -\gamma(V_N^*\Lambda^2 V_N U + 2V_N^*\Lambda V_N U V_N^*\Lambda V_N + UV_N^*\Lambda^2 V_N) + \theta(UV_N^*\Lambda V_N + V_N^*\Lambda V_N U) + B, \tag{4.7}$$

where B is the discrete matrix form of b. By defining $\bar{U} = V_N U V_N^*$ and $\bar{B} = V_N B V_N^*$ and multiplying V_N and V_N^* to the left-hand side and the right-hand side of (4.7), respectively, we further simplify the equation as

$$\bar{U} + \gamma(\Lambda^2\bar{U} + 2\Lambda\bar{U}\Lambda + \bar{U}\Lambda^2) - \theta(\Lambda\bar{U} + \bar{U}\Lambda) = \bar{B}. \tag{4.8}$$

Denote the left-hand side of (4.8) as $G(\bar{U})$. Since Λ is a diagonal matrix with entries λ_j, it can be verified that

$$g_{j,k} = (1 + \gamma(\lambda_j + \lambda_k)^2 - \theta(\lambda_j + \lambda_k))\bar{u}_{j,k} \quad \Longrightarrow \quad \bar{u}_{j,k} = \frac{\bar{b}_{j,k}}{g_{j,k}}. \tag{4.9}$$

Once $\bar{U}$ is obtained, it is easy to compute $U = V_N^* \bar{U} V_N$.

Note that the size of the stiff matrix M for the Laplace operator is $N \times N$ instead of sparse $N^2 \times N^2$ matrixes in the usual cases. As the eigenvalues λ_i can be prepared beforehand, the above computation can be made very efficient. Moreover, only the values U^k at p levels must be stored, with $2p \times N^2$ in total.

5. Efficiency enhancement with *p*-adaptivity. The time discretization using the energy convex splitting combined with the SDC scheme seems perfectly suitable for simulating the three phase-field models as it is of high order and is energy stable. Unfortunately, numerical instability is observed in large time numerical simulations, as demonstrated in Figure 4. The instability may be caused by the large number of corrections used. Without using corrections, the energy stability can be preserved but accuracy may not be satisfactory. However, using too many corrections may cause the above mentioned blow-up. It remains to balance the accuracy and stability. To this end, we will propose an adaptive strategy to adjust the correction number. Inspired by the idea in [31], we give a monitor function to predict the correction number at the $(n+1)$th step using the discrete energies $E_h(u^n)$ and $E_h(u^{n-1})$:

$$Np = \min\{N\max,\ \max\{0,\ N\max + \mathrm{fix}[\log_\eta(|E_h(u^n) - E_h(u^{n-1})| + \eta^{-(N\max+1)})]\}\}, \tag{5.1}$$

where η is a positive constant, $N\max$ is the maximum number of corrections, and fix$[\cdot]$ represents the integer part of a number.

Below we will explain the motivation of using (5.1) to predict Np. It is clear that more corrections are needed in the region where the energy decays fast. In other words, if the dynamical process evolves dramatically, then more corrections are required to capture the dynamical evolution correctly. More specifically, the relationship between Np and the energy change is given as follows:

$$Np = \begin{cases} 0 & \text{if} \quad |E_h(u^n) - E_h(u^{n-1})| < \eta^{-N\max,} \\ k & \text{if} \quad \eta^{-N\max+k} \le |E_h(u^n) - E_h(u^{n-1})| < \eta^{-N\max+k+1} \\ N\max & \text{if} \quad |E_h(u^n) - E_h(u^{n-1})| \ge \eta^{-1}, \end{cases} \tag{5.2}$$

where $N\max$ is upper bounded by $2p-1$ as the accuracy order of the interpolation on the $p+1$ Gauss–Radau nodes is $2p$ and the parameter η can be fixed as 3 or 5 in the later numerical tests.

Note that the physical energy decreasing property motivates us to use the energy difference at t_{n-1} and t_n for choosing the number of corrections. First, as observed from the energy curves in Figure 1, the energy variation in most time regimes is very small, so $Np = 0$ should be chosen in most of the time intervals. This implies that only the first-order SDC method is used, which guarantees the energy stability in general.

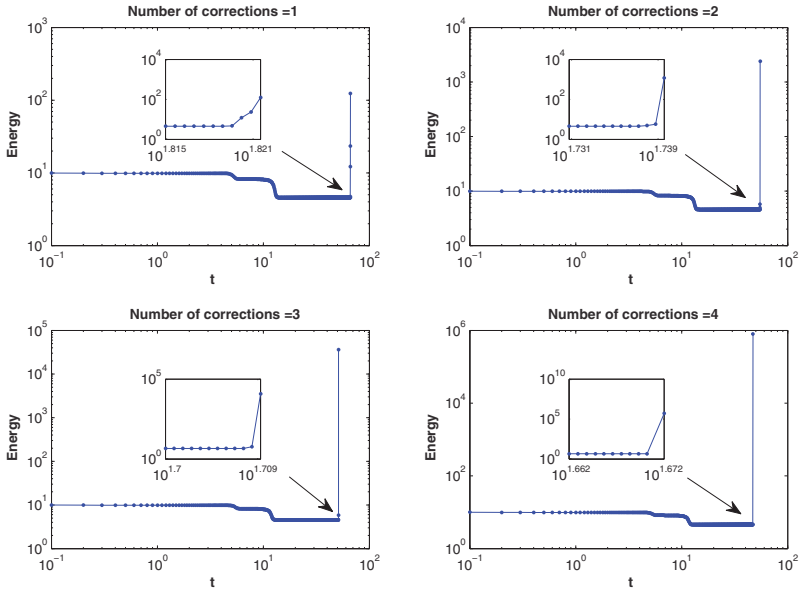

FIG. 4. *Example* 1*: Blow-up phenomenon for the SDC method with uniform number of corrections for long time simulation.*

Second, in the transition regime, the energy variation is between $\eta^{-N\max}$ and η^{-1}, which indicates some variable value of Np is used based on the size of the energy variation. Third, if the energy variation exceeds η^{-1}, then the maximum number of correction should be used. In the latter two cases, the energy decreasing property may not be preserved locally. However, as the total number of the intervals relevant to the last two cases is very small, it is expected that the overall energy stability can be preserved well. In other words, the choice of (5.2) seems very useful to balance the accuracy and overall energy stability.

6. Numerical experiments.

6.1. Convergence tests.

Example 6.1. We first test the convergence orders. To this end, consider the numerical solutions of the two-dimensional Allen–Cahn equation with $f(u) = u^3 - u$ and $\epsilon^2 = 0.01$. To verify the convergence order, we add a source term to the ACE such that the exact solution is

$$u(x, y) = \exp(-2t) \sin x \sin y, \quad (x, y) \in [0, 2\pi] \times [0, 2\pi].$$

We use the fast numerical solver proposed in section 4 for the spatial discretization and the semi-implicit SDC method for the time discretization. To test the numerical accuracy, we take a spatial grid of 600×600 with a coarse time step $dt = 0.4$. The L^2 norm error and L^∞ norm error at $T = 4$ with $p = 4$, $\beta = 1$, and $Np = 1, 2, 3, 4$, respectively, are shown in Table 1. It is observed that the numerical scheme with constant Np corrections in all time intervals gives an optimal order of accuracy in time.

6.2. SDC allows large time step. The following two examples are designed to study whether large time steppings are suitable for phase-field simulations.

Example 6.2. We will use the numerical example given in [39], i.e., we consider the Cahn–Hilliard equation with $f(u) = u^3 - u$ and $\epsilon^2 = 0.01$ with the initial condition

TABLE 1

Example 6.1*: Numerical errors and convergent rates against the number of corrections in the SDC method for the two-dimensional Allen–Cahn equation at* $T = 4$.

Np	Error	$dt = 0.4$	$dt/2$	$dt/4$
1	$\|u_{h,\tau} - u\|_2$	2.42	8.00e-1	2.15e-1
	Rate	/	1.59	1.8947
	$\|u_{h,\tau} - u\|_\infty$	5.46e-1	1.85e-01	4.97e-2
	Rate	/	1.56	1.90
2	$\|u_{h,\tau} - u\|_2$	4.76e-1	6.75e-2	8.87e-3
	Rate	/	2.82	2.93
	$\|u_{h,\tau} - u\|_\infty$	1.08e-1	1.52e-2	1.98e-3
	Rate	/	2.83	2.94
3	$\|u_{h,\tau} - u\|_2$	7.94e-2	5.69e-3	3.85e-4
	Rate	/	3.80	3.89
	$\|u_{h,\tau} - u\|_\infty$	1.77e-2	1.25e-3	8.45e-5
	Rate	/	3.82	3.89

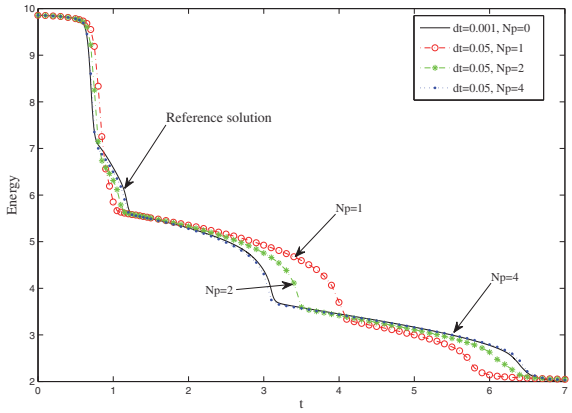

FIG. 5. *Example* 6.2*: Energy evolutions with different time steps and different numbers of corrections for the Cahn–Hilliard equation.*

$$u_0(x, y) = 0.05 \sin x \sin y, \qquad 0 \le x, y \le 2\pi,$$

and the periodic boundary condition.

We take the numerical solutions on a 400×400 mesh and the uniform time step $dt = 0.001$ as the "reference" solution. We fix $p = 4, \beta = 1$ and change $Np = 0, 1, 2, 4$ to implement the SDC methods. The energy evolution from $T = 0$ to 7 with different numbers of corrections are presented in Figure 5, where it is observed that the energy curves converge to the reference solution as the number of corrections increased even with a quite large time step $1/20$. When $Np = 4$, the energy curve almost coincides with the reference solution. In Figure 6, numerical solutions at $T = 2$ are obtained with $dt = 1/4$. It is well observed that the coarse stepsize together with four or five corrections can significantly improve the quality of the approximation.

Example 6.3. This example uses large time steps to simulate the thin film models without slope selection. We take the same initial condition, boundary condition, and physical parameters as in Example 6.2, but the energy potential is given by (1.12).

We use the same computational grids both in time and in space as in Example 6.2 but the parameter β in the numerical scheme (2.14) is chosen to be 0.5. Convergence with respect to the number of corrections is shown in Figure 7.

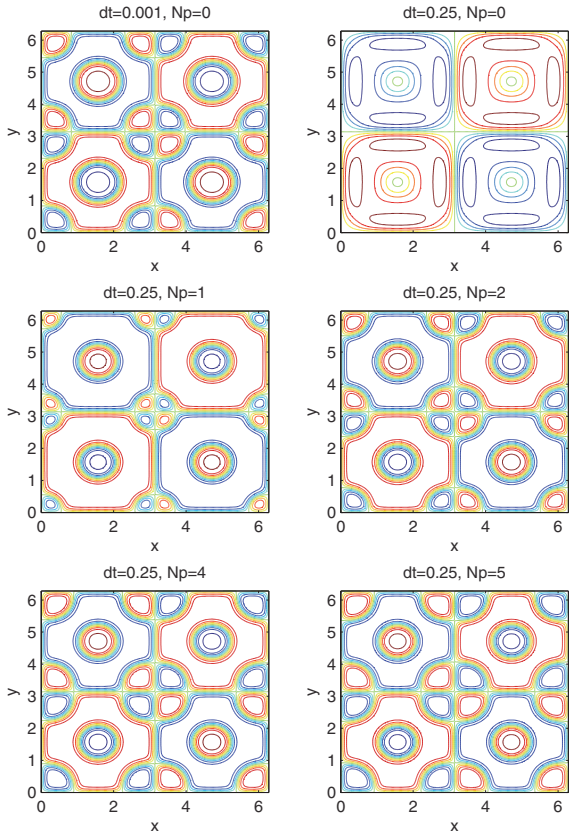

FIG. 6. *Example* 6.2*: Numerical solutions for the Cahn–Hilliard equation at time* $T = 2$ *using the SDC method.*

6.3. Long time simulation by the adaptive SDC method. It is observed from Figures 5–7 that large time steps with some corrections can indeed improve the solution accuracy and also capture the dynamical solution correctly. However, as demonstrated in Figure 3, the balance of accuracy and energy stability does not hold for larger T. This requires the use of an adaptive approach.

Example 6.4. We will use the adaptive SDC scheme for long time simulation of the Cahn–Hilliard equation with initial condition

$$u_0(x, y) = 0.05 \sin x \sin y + 0.001, \qquad 0 \le x, y \le 2\pi,$$

and the periodic boundary condition. The parameter ϵ^2 is chosen as 0.01.

The mesh grid in space is fixed as 400×400. We take the numerical solutions with small uniform time step $dt = 0.001$ as the "reference" solution. We take $p = 4$ in the SDC method, and $\beta = 1$ in (2.17), $\eta = 5, N\max = 5$ in (5.2), and set $Np = N\max$ at the first step. Then we use the monitor function to update Np afterward. The energy curves and the numerical results are showed in Figures. 8–11.

In Figure 8, with the adaptive SDC scheme we can use $dt = 0.04$ to obtain a nearly coincident energy curve as that for $dt = 0.001$ without adaptivity. On the other hand, the energy curve will be far from the reference energy cureve if we use $dt = 0.04$ without adaptivity, especially before $T = 10$, which can be seen in the

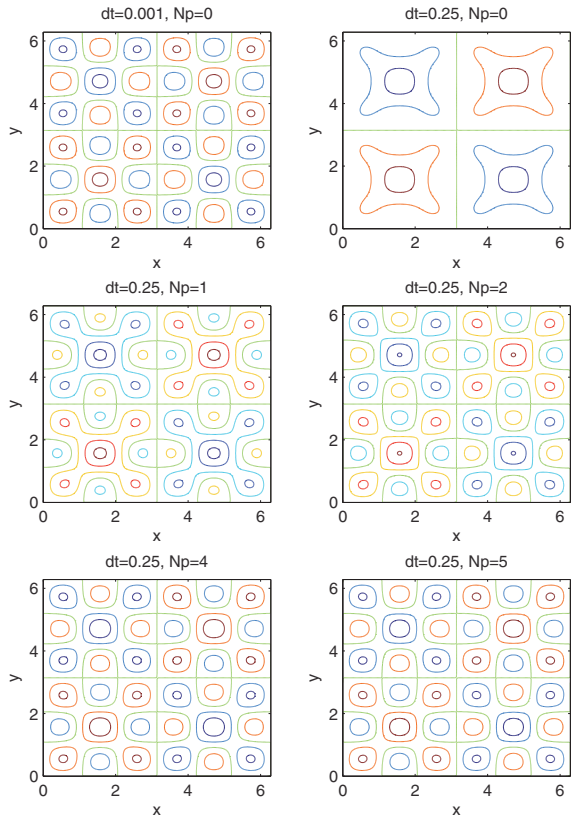

FIG. 7. *Example* 6.3*: Numerical solutions of the thin film model without slope selection at time* $T = 2$ *using different numbers of iterations. It is seen that with five iterations,* $dt = 0.25$ *gives almost the same results as the* $dt = 10^{-3}$ *results.*

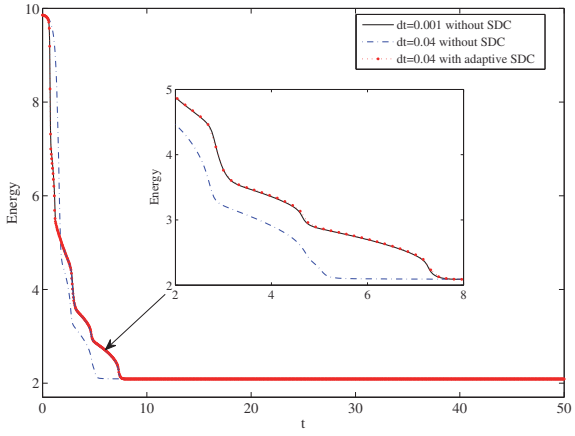

FIG. 8. *Example* 6.4*: Energy curves of the Cahn–Hilliard equation by different schemes with different time steps.*

locally magnified energy curves from $T = 2$ to 8. The number of iterations used in each time step is plotted in Figure 9, where as expected the larger slope of the energy

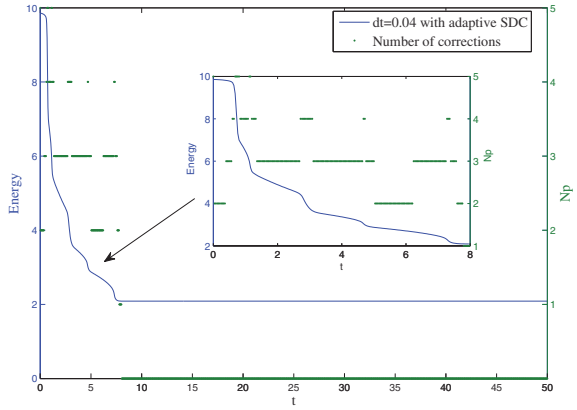

FIG. 9. *Example* 6.4*: Energy curves of the Cahn–Hilliard equation (left y-axis) and number of corrections (right y-axis) by the adaptive SDC schemes.*

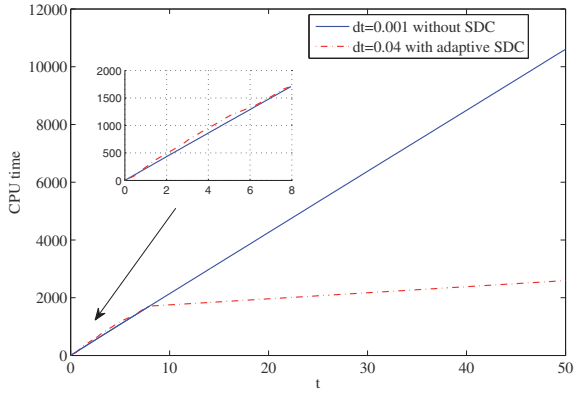

FIG. 10. *Example* 6.4*: CPU time comparison between different schemes for the Cahn–Hilliard equation.*

curve corresponds to a bigger number of corrections. The CPU time comparison is presented in Figure 10, where it is seen that our adaptive SDC scheme consumes more CPU time at the beginning as more corrections are needed to capture the fast dynamical evolution. However, our adaptive SDC scheme can enhance the efficiency significantly in the long time computation. The numerical solutions at different time levels are presented in Figure 11, where it is observed that the solution dynamics can be captured correctly with larger time steps when an adaptive strategy is employed.

Example 6.5. Consider the thin film model with slope selection with $f(\nabla u) = (1 - |\nabla u|^2)\nabla u$ as given in [27] with the initial value

$$u_0 = 0.1(\sin 3x \sin 2y + \sin 5x \sin 5y)$$

and the periodic boundary condition. The parameter ϵ^2 is 0.1 and the computation domain is $\Omega = [0, 2\pi] \times [0, 2\pi]$.

The spatial space is divided into a 400×400 mesh. We fix $p = 3, \beta = 2$ and set $\eta = 3$ and $Np = 5$ at the first time step. We take the numerical result by the convex splitting schemes without SDC with time step $dt = 0.001$ as the "reference" solution. The energy evolutions and the number of corrections are shown in Figures 12 and 13,

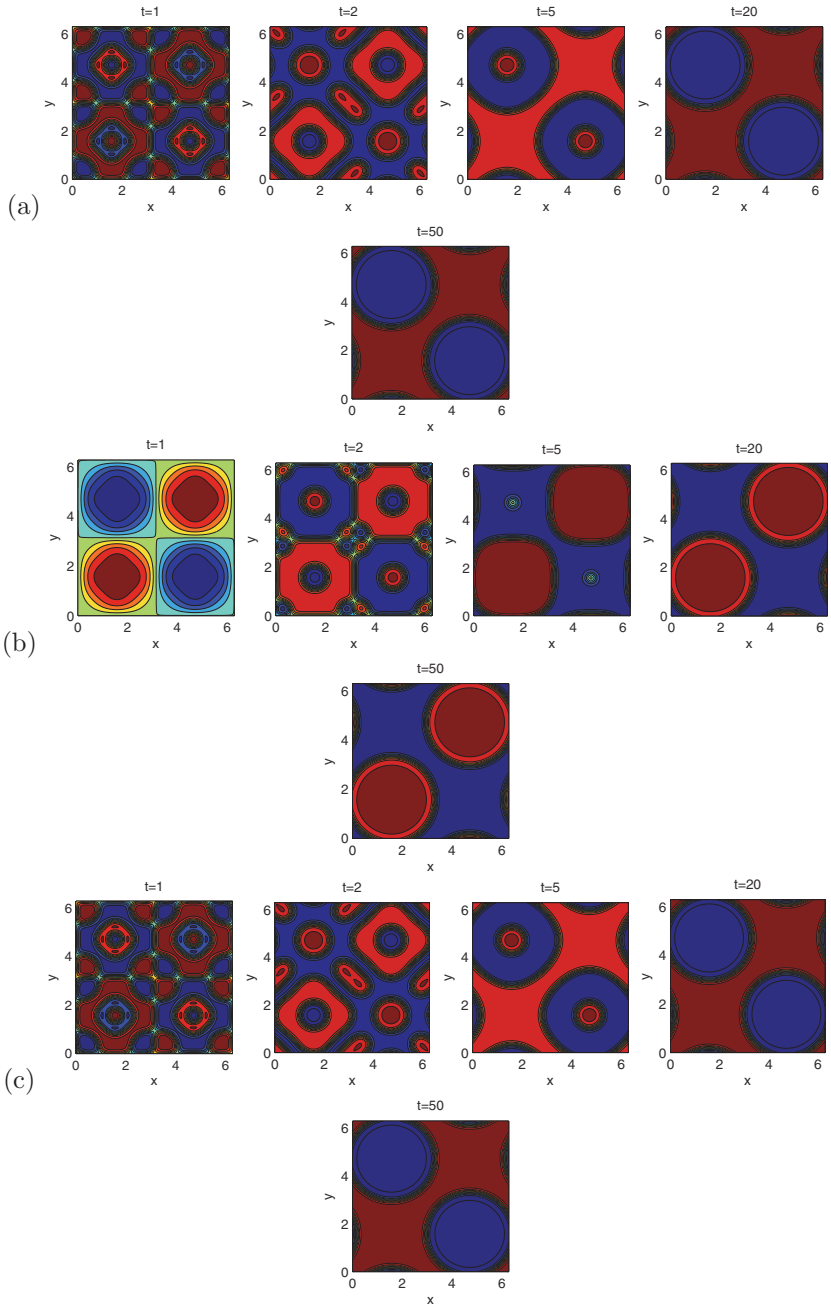

FIG. 11. *Example* 6.4*: Solution variation at different times, using* (a) *the direct energy convex splitting scheme without SDC and* $dt = 0.001$*;* (b) *the direct energy convex splitting scheme without SDC and* $dt = 0.04$*; and* (c) *the adaptive SDC scheme with* $dt = 0.04$.

respectively. We can see from Figure 12 that the energy curve obtained by the adaptive SDC scheme with $dt = 0.02$ is in good agreement with the reference curve, while the difference between the $dt = 0.001$ and $dt = 0.02$ curves, both without adaptivity,

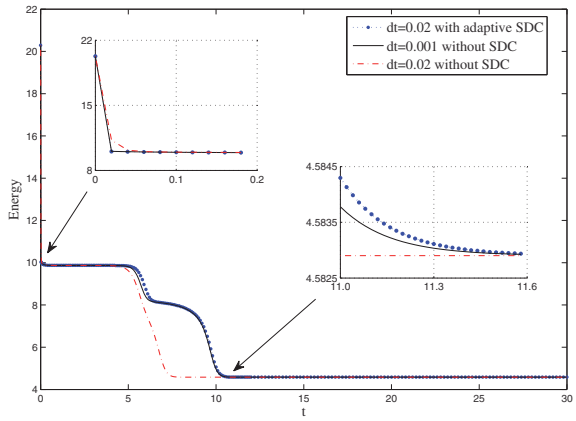

FIG. 12. *Example* 6.5*: Energy curves of the thin film with slope selection by different schemes with different time steps.*

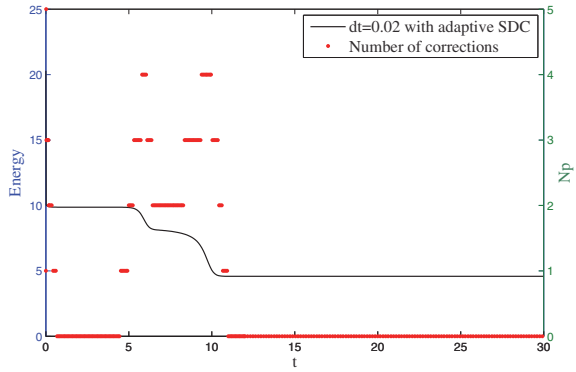

FIG. 13. *Example* 6.5*: Energy curves of the thin film model with slope selection (left y-axis) and number of corrections (right y-axis) by the adaptive SDC schemes.*

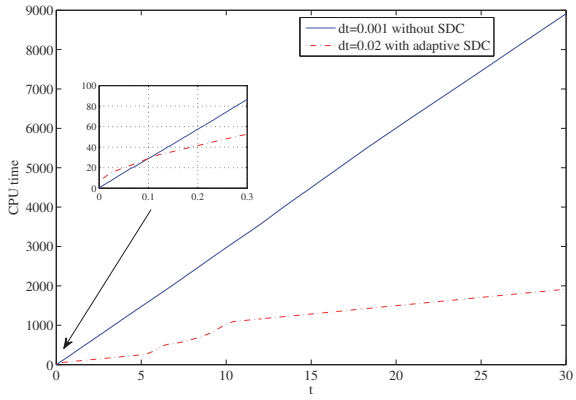

FIG. 14. *Example* 6.5*: CPU time comparison between different schemes for the thin film model with slope selection.*

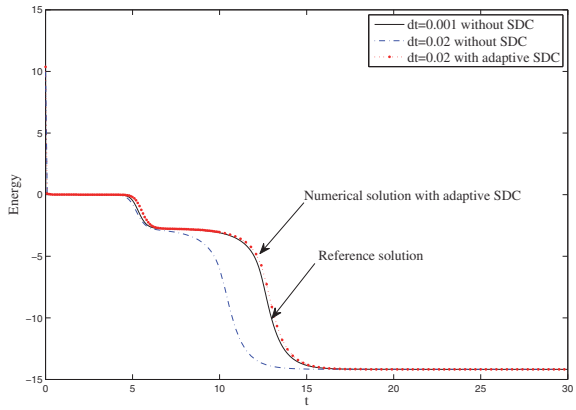

FIG. 15. *Example* 6.6*: Energy curves of the thin film without slope selection by different schemes with different time steps.*

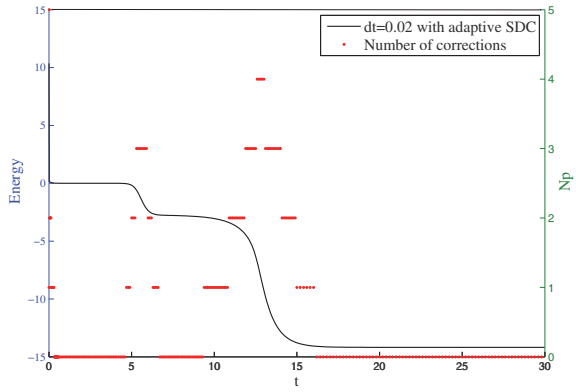

FIG. 16. *Example* 6.6*: Energy curves of the thin film model without slope selection (left y-axis) and number of corrections (right y-axis) by the adaptive SDC schemes.*

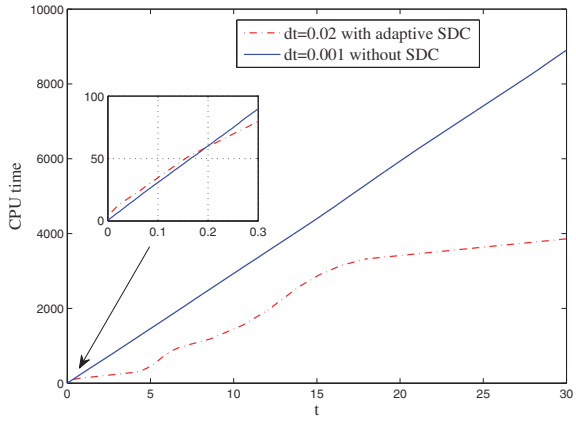

FIG. 17. *Example* 6.6*: CPU time comparison between different schemes for the thin film model without slope selection.*

is very big. It is also observed from Figure 13 that the number of corrections is proportional to the slope of the energy curve. In Figure 14, the CPU time comparison is made, and it is clearly seen that the adaptive computation can indeed enhance the efficiency.

Example 6.6. Consider the thin film model without slope selection with $f(\nabla u) = -\frac{\nabla u}{1+|\nabla u|^2}$ as given in [27] with the same initial values as Example 6.5.

We fix $\beta = 0.5$ and $\eta = 5$ and set the same values as in Example 6.5 for other parameters at the first time step. Similarly we obtain satisfactory numerical results as plotted in Figures 15 and 16 and the CPU time improvement as plotted in Figure 17.

To test the robustness of the parameters, we also tried $\eta = 2$ and $\eta = 7$ in the above two examples. In both cases, the corresponding numerical results are also satisfactory.

7. Concluding remarks. In this paper, a temporal p-adaptive scheme based on energy convex splitting is designed for solving the phase-field models. The p-adaptivity is realized by employing the SDC method at some needed time levels. In space, we first use a fast solver for the Laplace operator and then use the DFT matrix technique to diagonalize the resulting circulant linear system. This approach highly enhances the overall solution efficiency.

We aim to balance the accuracy and stability by using the p-adaptive scheme. To this end, a practical strategy is proposed to control the number of the corrections based on the variation of the energy curve. This turns out to be a simple and effective approach.

Numerical experiments demonstrate that the proposed p-adaptive scheme is very effective for solving the phase-field models. It can enhance accuracy of the numerical solution by increasing the number of corrections to capture the fast time scale dynamics and also save computational time by using a lower-order method for slow dynamics. With the p-adaptive technique, much larger time steps (e.g., dt=1/25) can be used to catch both solution dynamics and steady states.

REFERENCES

[1] S. M. Allen and J. W. Cahn, *A microscopic theory for antiphase boundary motion and its application to antiphase domain coarsening*, Acta Metallurgica, 27 (1979), pp. 1085–1095.

[2] P. Aviles and Y. Giga, *A mathematical problem related to the physical theory of liquid crystal configurations,* Proc. Centre Math. Anal. Austral. Nat. Univ., 12 (1987), pp. 1–16.

[3] J. M. Ball and R. D. James, *Proposed experimental tests of a theory of fine microstructure and the two-well problem*, Philos. Trans. R. Soc. Lond. Ser. A, 338 (1992), pp. 389–450.

[4] A. L. Bertozzi, S. Esedoglu and A. Gillette, *Inpainting of binary images using the Cahn-Hilliard equation,* IEEE Trans. Image Process, 16 (2007), pp. 241–266.

[5] J. W. Cahn and J. E. Hilliard, *Free energy of a nonuniform system,* I*: Interfacial free energy,* J. Chem. Phys., 28 (1958), pp. 258–267.

[6] F. Chen and J. Shen, *Efficient energy stable schemes with spectral discretization in space for anisotropic Cahn-Hilliard systems*, Commun. Comput. Phys., 13 (2013), pp. 1189–1208.

[7] L.-Q. Chen, *Phase-field models for microstructural evolution*, Ann. Rev. Mater. Res., 32 (2002), pp. 113–140.

[8] W. Chen, S. Conde, C. Wang, X. Wang, and S. M. Wise, *A linear energy stable scheme for a thin film model without slope selection,* J. Sci. Comput., 52 (2012), pp. 546–562.

[9] W. Chen, C. Wang, X. Wang, and S. M. Wise, *A linear iteration algorithm for an energy stable second-order scheme for a thin film model without slope selection*, J. Sci. Comput., 59 (2014), pp. 579–601.

[10] A. Christlieb, B. Ong, and J. Qiu, *Spectral deferred correction methods with high order Runge-Kutta schemes in prediction and correction steps*, Commun. Appl. Comput. Math., 4 (2009), pp. 27–56.

[11] C. Collins, J. Shen, and S. M. Wise, *An efficient, energy stable scheme for the Cahn-Hilliard-Brinkman system*, Commun. Comput. Phys., 13 (2013), pp. 929–957.

[12] P. J. Davis, *Circulant Matrices*, 2nd ed., Chelsea, New York, 1994.
[13] Q. Du and R. A. Nicolaides, *Numerical analysis of a continuum model of phase transition,* SIAM J. Numer. Anal., 28 (1991), pp. 1310–1322.
[14] A. Dutt, L. Greengard, and V. Rokhlin, *Spectral deferred correction methods for ordinary differential equations,* BIT, 40 (2000), pp. 241–266.
[15] C. M. Elliott and B. Stinner, *Computation of two-phase biomembranes with phase dependent material parameters using surface finite elements*, Commun. Comput. Phys., 13 (2013), pp. 325–360.
[16] H. Emmerich, *The Diffuse Interface Approach in Materials Science*, Springer, New York, 2003.
[17] D. J. Eyre, *An Unconditionally Stable One-Step Scheme for Gradient Systems*, (1998). http://www. math.utah.edu/eyre/research/methods/stable.ps
[18] X. Feng, H. Song, T. Tang, and J. Yang, *Nonlinearly stable implicit-explicit methods for the Allen-Cahn equation*, Inverse Probl. Imaging, 7 (2013), pp. 679–695.
[19] X. Feng, T. Tang, and J. Yang, *Stabilized Crank-Nicolson/Adams-Bashforth schemes for phase field models*, East Asian J. Appl. Math., 3 (2013), pp. 59–80.
[20] D. Furihata, *A stable and conservative finite difference scheme for the Cahn-Hilliard equation,* Numer. Math., 87 (2001), pp. 675–699.
[21] L. Golubovic, A. Levandovsky, and D. Moldovan, *Interface dynamics and far-from-equilibrium phase transitions in multilayer epitaxial growth and erosion on crystal surfaces: Continuum theory insights,* East Asian J. Appl. Math., 1 (2011), pp. 297–371.
[22] H. Gomez and T. J. R. Hughes, *Provably unconditionally stable, second-order time-accurate, mixed variational methods for phase-field models,* J. Comput. Phys., 230 (2011), pp. 5310–5327.
[23] Y. He, Y. Liu, and T. Tang, *On large time-stepping methods for the Cahn-Hilliard equation,* Appl. Numer. Math., 57 (2007), pp. 616–628.
[24] A. Kassam and L. N. Trefethen, *Fourth-order time-stepping for stiff PDEs,* SIAM J. Sci. Comput., 26 (2005) pp. 1214–1233.
[25] J. Kim, *Phase-field models for multi-component fluid flows,* Commun. Comput. Phys., 12 (2012), pp. 613–661.
[26] R. Kohn and S. Müller, *Surface energy and microstructure in coherent phase transitions,* Comm. Pure Appl. Math., 47 (1994), pp. 405–435.
[27] B. Li and J. G. Liu, *Thin film epitaxy with or without slope selection,* European J. Appl. Math., 14 (2003), pp. 713–743.
[28] F. Liu and J. Shen, *Stabilized semi-implicit spectral deferred correction methods for Allen-Cahn and Cahn-Hilliard equations,* Math. Methods Appl. Sci.
[29] M. Minion, *Semi-implicit spectral deferred correction methods for ordinary differential equations,* Commun. Math. Sci., 1 (2003), pp. 471–500.
[30] O. Penrose and P. C. Fife, *Thermodynamically consistent models of phase-field type for the kinetics of phase transition,* Phys. D, 43 (1990), pp. 44–62.
[31] Z. Qiao, Z. Zhang, and T. Tang, *An adaptive time-stepping strategy for the molecular beam epitaxy models,* SIAM J. Sci. Comput., 33 (2011), pp. 1395–1414.
[32] J. Shen, T. Tang, and L. Wang, *Spectral Methods: Algorithms, Analysis and Applications*, Springer Ser. Comput. Math. 41, Springer, New York, 2011.
[33] J. Shen, C. Wang, S. Wang, and X. Wang, *Second-order convex splitting schemes for gradient flows with Ehrlich-Schwoebel type energy: Application to thin film epitaxy,* SIAM J. Numer. Anal, 50 (2012), pp. 105–125.
[34] J. Shen and X. Yang, *Numerical approximations of Allen-Cahn and Cahn-Hilliard equations,* Discrete Contin. Dyn. Syst., 28 (2010), pp. 1669–1691.
[35] T. Tang, H. Xie, and X. Yin, *High-order convergence of spectral deferred correction methods on general quadrature nodes*, J. Sci. Comput., 56 (2012), pp. 1–13.
[36] J. D. van der Waals, *The thermodynamic theory of capillarity under the hypothesis of a continuous variation of density,* J. Stat. Phys., 20 (1979), pp. 197–244.
[37] C. Wang, X. Wang, and S. M. Wise, *Unconditionally stable schemes for equations of thin film epitaxy*, Discrete Contin. Dyn. Syst. A, 28 (2010) pp. 405–423.
[38] C. Xu and T. Tang, *Stability analysis of large time-stepping methods for epitaxial growth models,* SIAM J. Numer. Anal., 44 (2006), pp. 1759–1779.
[39] Z. Zhang and Z. Qiao, *An adaptive time-stepping strategy for the Cahn-Hilliard equation*, Commun. Comput. Phys., 11 (2011), pp. 1261–1278.